

# Correlation induced emergent charge order in metallic vanadium dioxide

Christopher N. Singh,<sup>1,\*</sup> L. F. J. Piper,<sup>1</sup> Hanjong Paik,<sup>2</sup> Darrell G. Schlom,<sup>3,4</sup> and Wei-Cheng Lee<sup>1,†</sup>

<sup>1</sup>*Department of Physics, Applied Physics, and Astronomy,  
Binghamton University, Binghamton, New York 13902, USA*

<sup>2</sup>*Department of Materials Science and Engineering,  
Cornell University, Ithaca, New York 14853-1501, USA*

<sup>3</sup>*Department of Materials Science and Engineering,  
Cornell University, Ithaca, New York 14853-1501, USA*

<sup>4</sup>*Kavli Institute at Cornell for Nanoscale Science, Ithaca, New York 14853, USA*

(Dated: May 7, 2020)

Recent progress in growth and characterization of thin-film VO<sub>2</sub> has shown its electronic properties can be significantly modulated by epitaxial matching. To throw new light on the concept of ‘Mott engineering’, we develop a symmetry-consistent approach to treat structural distortions and electronic correlations in epitaxial VO<sub>2</sub> films under strain, and compare our design with direct experimental probes. We find strong evidence for the emergence of correlation-driven charge order deep in the metallic phase, and our results indicate that exotic phases of VO<sub>2</sub> can be controlled with epitaxial stabilization.

**Introduction** — The nature of the metal-insulator transition (MIT) in VO<sub>2</sub> has far reaching implications for both fundamental physics [1–4] and blossoming applications in neuromorphic computing [5–9]. From a fundamental viewpoint, the correlation effects of 3*d* orbitals in transition metal oxides exhibit rich ground state properties ranging all the way from metallic ferromagnets to wide-gap semi-conductors [10, 11]. For instance, the MIT in VO<sub>2</sub> is near room temperature, but the isoelectronic compound, NbO<sub>2</sub>, has a transition temperature orders of magnitude higher [12, 13], and TiO<sub>2</sub> lacks a transition entirely [14]. The origin of the MIT in VO<sub>2</sub> remains contested [15] after years of study because neither a Peierls [10, 16, 17] nor a Mott picture align entirely with all the experimental evidence [18–24]. The scenario where a Peierls distortion and Mott physics cooperatively lead to the MIT has also been investigated extensively [25–31]. Resolving this issue has become even more pressing with the advent of vanadium based memristor technologies [32–35] that could exploit Mott transitions for beyond von Neumann computing [36]. While the resistivity switching in these new memristors is achieved by driving in a non-equilibrium thermal environment, disputes remain as to the origin of the switching [37]. This situation has redirected massive experimental efforts towards understanding epitaxial VO<sub>2</sub> thin films using TiO<sub>2</sub> substrates, which offer the possibility of enhancing electron correlation effects with severe strain even before the Peierls distortion [38–44].

TiO<sub>2</sub> is a wide-gap system ( $\sim 3.2\text{eV}$ ) with a stable rutile crystal structure at all temperatures, making it an excellent substrate for VO<sub>2</sub> thin film engineering. Because the *c*-axis lattice constant of TiO<sub>2</sub> is  $\sim 3.8\%$  longer than bulk VO<sub>2</sub>, strain effects in epitaxial VO<sub>2</sub> films can be modulated by choosing the growth direction on TiO<sub>2</sub>

substrates. It has been observed that if the growth direction is perpendicular to the rutile *c*-axis, e.g., VO<sub>2</sub> [100] and VO<sub>2</sub> [110], the elongation of *c*-axis of VO<sub>2</sub> due to strain gives rise to stronger correlation effects, resulting in a number of new phases including the intermediate insulating M<sub>2</sub> phase [42], an orbital selective Mott state [41], and the enhancement of the lower Hubbard band [43]. These results demonstrate that VO<sub>2</sub> thin films are a unique platform for ‘Mott engineering’, and can exhibit richer correlation effects not observed in bulk VO<sub>2</sub>. However, a theoretical description of the interplay between strain and electron correlation is still far from complete [45]. A definitive theoretical treatment of VO<sub>2</sub> across different thin film growth orientations within a common group representation is necessary to address important questions such as effects of lattice symmetry breaking on electron-electron correlation, phase diagrams of emerging electron states of matter, etc. In particular, the theoretical framework has to address how lattice and orbital degrees of freedom are influenced in thin films where geometrical degeneracies are lifted by strain [46–48].

In this Letter we determine the Bravais system that seamlessly connects different strain conditions in VO<sub>2</sub> grown on TiO<sub>2</sub> substrates, and employ density functional theory with appropriate functionals that capture all relevant features of the MIT in VO<sub>2</sub> including the gap, magnetic order, energy hierarchy, et cetera [49–51]. With this methodology, we are able to study systematically the evolution of correlation effects under different strains. We show that our first principles atomistic models reproduce accurately the experimental results of O K-edge x-ray absorption spectrum (XAS) in VO<sub>2</sub> [001], VO<sub>2</sub> [100], VO<sub>2</sub> [110]. As XAS is often used to detect charge disproportionation [52, 53], we contrast our theory against experiment and find strong evidence that in highly strained systems, a novel electronic charge order (CO) emerges in the metallic rutile phase before the structural transition occurs, due directly to the interplay between electron-

\* csingh5@binghamton.edu

† wlee@binghamton.edu

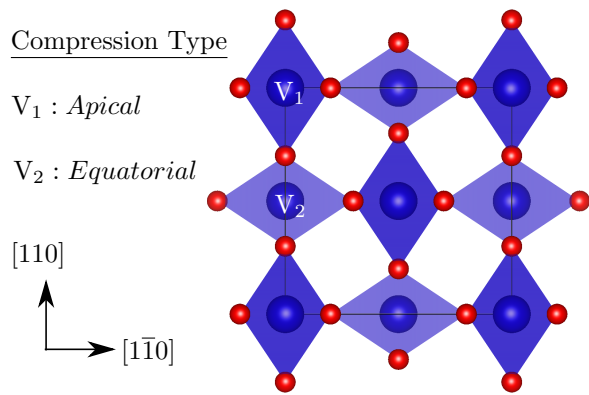


FIG. 1. (Color online) Rutile VO<sub>2</sub> shown in transformed basis. [110] growth effects the two vanadium positions differently by modulating either apical or equatorial bond distances. Image by VESTA [54]

electron correlation and local symmetry breaking arising from strain. This CO naturally leads to two independent vanadium positions inside the rutile unit cell, paving the way for the occurrence of M<sub>2</sub> phase observed in previous experiments [42]. Our results demonstrate that strain-engineered VO<sub>2</sub> thin films are a unique correlated system allowing tunable Mott correlation and a rich phase diagram featuring a strongly correlated metal.

**Methods** — Using TiO<sub>2</sub> as a substrate, there are several possible growth orientations for VO<sub>2</sub> [55]. The growth and measurement techniques employed in this work are detailed in Refs. [39] and [40–42]. Here we will adhere to the standard naming scheme where a Miller index in the rutile basis denotes the common vector between both film and substrate, and is normal to the interface. This uniquely defines the considered growth directions ([001], [100], and [110]). Because many first principles approaches implement symmetry mapping operations to conserve computation, and because we want to cross-compare simulations in different point groups, we determine space group 6 (*Pm*) as the lowest common Bravais lattice for the [001], [100], and [110] films. This ensures that no artificial symmetry is enforced or broken in the simulation while the self-consistency condition is reached. A similar approach has been applied in the sister compound NbO<sub>2</sub> to investigate structural effects across a metal to insulator transition [56].

The lattice parameters for the [001] and [100] growth orientations can be calculated straightforwardly in the original rutile atomic basis because it is commensurate with the rutile TiO<sub>2</sub> symmetry, however, in order to simulate the [110] growth condition, a linear map is applied to the VO<sub>2</sub> basis defined by

$$\mathcal{M} = \begin{pmatrix} 1 & 1 & 0 \\ -1 & 1 & 0 \\ 0 & 0 & 1 \end{pmatrix}. \quad (1)$$

This defines the growth direction along the crystallo-

graphic *b*-axis as shown in Fig. 1. If the volume of bulk VO<sub>2</sub> is  $\Omega$ , the growth direction lattice vector of VO<sub>2</sub> can be determined as

$$a_3^{\text{VO}_2} = \frac{\Omega}{a_1^{\text{TiO}_2} \cdot a_2^{\text{TiO}_2}}. \quad (2)$$

In Eqn. 2 the numerical subscripts can be permuted as needed to represent the out of plane direction depending on the growth orientation. To determine the new lattice vectors, the same map  $\mathcal{M}$  is applied to the TiO<sub>2</sub> lattice vectors, the in plane vectors are matched, and the out of plane vector is determined with Eqn. 2. Then the inverse map  $\mathcal{M}^{-1}$  is applied. This procedure keeps the atomic basis the same, but may change the lattice vectors and the angles. The experimental film characterization is given in Ref. [42] and the parameters used in the simulation are given in Table I.

TABLE I. Lattice parameters used in strain simulation.

Parameter	Bulk	[001]	[100]	[110] <sup>a</sup>
<i>a</i> (Å)	4.55460	4.59330	4.35141	4.47399
<i>b</i> (Å)	4.55460	4.59330	4.59330	4.47399
<i>c</i> (Å)	2.85140	2.80355	2.95940	2.95940

<sup>a</sup> In this case the monoclinic angle is  $\gamma \approx 93.1^\circ$

The electronic structure simulations were performed within the WIEN2k [57] ecosystem. In the occupation number calculations, a 20,000 kpoint sampling was used with an RKmax of 7.2. The RMT's were fixed to 1.82 and 1.65 a.u for vanadium and oxygen respectively, and the GMAX was set to 14. This is necessary so that the mixed basis sets used in the computation are consistent. The functional used was either PBE [58], mBJ [59], or SCAN [60]. Spin orbit coupling is known to be a negligible energy scale, and no magnetic ordering was stabilized.

Being that quantum mechanics only defines a continuous charge density distribution, the definition of how much charge is assigned to a specific atom is a subtle question [61] that has been approached in many ways. For example, Mulliken [62], Bader [63], and Hirshfeld [64] all have well known methods. We choose here the density matrix formalism. In the full-potential-linear-augmented-plane-wave method [65], the Kohn-Sham eigenfunctions  $|\psi_i\rangle$  have some components that are atomic-like and can be written as linear combinations of spherical harmonics in the usual way  $|lm\sigma\rangle$ . These are defined inside a radial basin of radius  $R_{MT}$ . Defining the density matrix as

$$\hat{n}_{lmm'\sigma\sigma'} = \sum_{\varepsilon_i \leq E_f} \langle lm'\sigma' | \psi_i \rangle \langle \psi_i | lm\sigma \rangle, \quad (3)$$

the density of electrons in the *d* level  $n_d$  can be calculated by tracing out the orbitals as  $\text{Tr}[\hat{n}_d]$ . This allows for a quantitatively consistent definition of the radial wavefunction assigned to each atomic site across all structural phases. In this way, the amount of charge around a given atom is consistently monitored as the strain is applied.

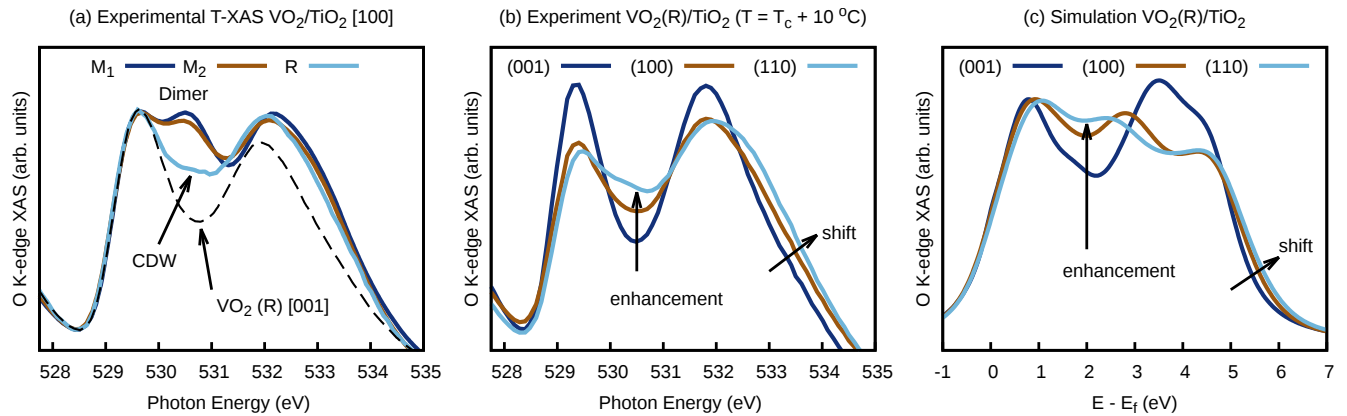


FIG. 2. (Color online) **Strain induced spectral evolution** (a) Adapted from Quackenbush et. al [42], the temperature dependence of oxygen K-edge across the transitions show that dimerization is differentiable from charge/orbital ordering by comparing against  $\text{VO}_2$  (R) [001] (dashed line). (b) The enhancement in the peak at  $\approx 530.5$  eV compared to the bulk phase is a signature of inequivalent vanadium positions [42], and the corresponding vanadium L-edge has been used to show strain induced orbital selectivity [43]. The measurement was taken deep inside the metallic state, and yet signatures of vanadium differentiation are observed, providing strong evidence for the onset of correlation stabilized charge order. (c) mBJ level simulation of  $\text{VO}_2$ (R) oxygen K-edge demonstrating response of electronic structure to strain results in experimentally observed spectral features.

In defining the  $d$  orbitals, we follow the conventions laid down in the seminal work by Eyert [10]. Because there are two different local octohedral environments for vanadium with respect to the global crystallographic system as shown in Fig. 1, the convention is to orient the local coordinate systems such that the  $z$  axis points along either the [110] or the  $[1\bar{1}0]$  directions for  $V_2$  and  $V_1$  respectively. This choice ensures the  $d_{xy}$  and the  $d_{z^2}$  orbitals form the  $e_g$  manifold and lie higher in energy than the remaining three that form the  $t_{2g}$  manifold.

**Results** — The effect on the electronic structure in response to lattice symmetry breaking is found by contrasting the experimental and simulated XAS summarized in Fig. 2. While it is well known the 530.5 eV peak is enhanced in the  $M_2$  phase relative to the rutile phase [42], and the  $M_2$  phase is known to have two inequivalent vanadium sites, we stress this is not an observation of the  $M_2$  phase as evidenced by Fig. 2a. In Fig. 2b, different growth orientations within the rutile phase (the measurement was performed well above the transition temperature in high quality films) enhance the 530.5 eV spectral feature — a strong fingerprint that vanadium differentiation has developed. One might expect that since the [110] growth orientation can break the  $V_1$ - $V_2$  equivalency directly, the observed features are simply a result of lattice symmetry breaking, however, as is shown in Fig 3b, without considering non-local correlations, there is no splitting in the spectral function of unoccupied states. This means the spectral weight transfer is a direct result of lattice and correlation interplay that is strongly enhanced in the [110] growth, because neither alone can reproduce experiment. We additionally see similar effects in the [100] growth orientation where explicit lattice symmetry breaking does not occur, but spectral signatures of

correlation enhancement persist [43, 44]. Ultimately, the evolution of the XAS waveform represents an experimental signature that non-local correlations have broken the equivalence between the two vanadium sites in the rutile phase, and the spectral features are quantitatively reproduced by a first principles analysis.

Figure 3b shows the density of states for the  $t_{2g}$  manifold where it is observed that [110] epitaxial growth modifies the  $d \cdot p$  orbital hybridization differently for  $V_1$  and  $V_2$ . For the octohedra oriented along the growth direction, the apical bond distance is shortened. For  $V_1$ , the  $d_{xz}$  orbital lies along this compressed axis, increasing the hybridization as pushing the energy higher. The opposite effect is seen for  $V_2$ , where because the  $d_{xz}$  is rotated 90° about the rutile  $c$ -axis, the hybridization is decreased relative to the unstrained sample, ultimately lowering the onsite energy. For the other four  $d$  orbitals, the  $V_1$  spectral function is lowered, while the  $V_2$  spectral function is raised in energy. The high energy  $e_g$  manifold is not shown because the weight at the chemical potential of these orbitals is small. One can see however that even in the strained case, the  $t_{2g}$  weight at the Fermi level is roughly equal for each vanadium at the GGA level. However, with a functional that correctly predicts every other facet of  $\text{VO}_2$  such as mBJ [49], we find charge order developing in the low lying manifold, and the only assumption we drop that others have made, is that  $V_1$  is strictly equivalent to  $V_2$  in strained metallic samples. This redistribution of spectral weight has the additional consequence of modulating orbital occupation as shown in Fig. 3c, where we show that another semi-local approximation containing a kinetic energy density term such as SCAN enhances the difference between the two vanadium sites. We conclude even though symmetry breaking can

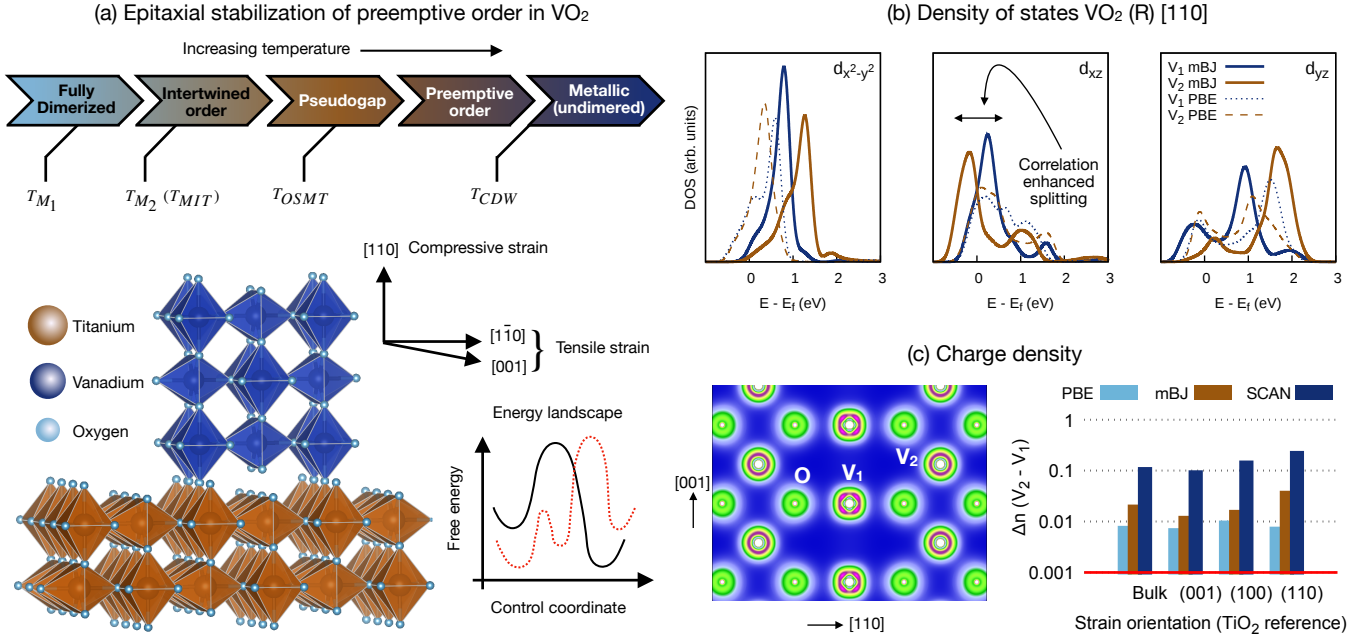


FIG. 3. (Color online) **Strain engineering VO<sub>2</sub>** (a) A proposed phase diagram of VO<sub>2</sub> is shown with preemptive charge ordering occurring before Peierls transition where charge/orbital ordering is accessed through epitaxial stabilization. The crystal structure shows the interfacial relation between TiO<sub>2</sub> and VO<sub>2</sub> octohedra and the resulting strain vectors. (b) The low lying vanadium *d* manifold is split in the strained case by non-local correlations (mBJ). The PBE result for is shown as dashed lines, where even in the presence of lattice symmetry breaking, there is negligible difference between V<sub>1</sub> and V<sub>2</sub> at the Fermi energy. (c) A charge density map shows density differentiation (mBJ level), and the bar plot shows the occupation difference between the two vanadium sites averaged over different volume conservation conditions. Non-local correlations enhance the difference, as do (100) and (110) growth conditions, demonstrating the Mott condition can be engineered by strain

occur at the level of the lattice, the electron-ion dynamics in VO<sub>2</sub> are deeply intertwined, and that correlation effects can stabilize a previously undiscovered charge order in metallic VO<sub>2</sub>.

**Discussion** — Our theoretical and experimental results support the cooperative scenario for VO<sub>2</sub> that both structural distortion and electron correlation are important for the MIT mechanism. In the metallic rutile phase, although the structural changes due to strain have large effects on the electronic properties, this is not sufficient to satisfy the Mott criterion and induce a Mott transition. Nevertheless, electron-electron interactions are still very important, and the emergence of charge order in the phase diagram of VO<sub>2</sub> films discovered here echoes the charge density wave states observed in various correlated materials including high-temperature cuprate superconductors [66–70] and transition metal dichalcogenides [71]. Moreover, we find that phases observed in VO<sub>2</sub> thin films can be nicely understood as intertwined orders between the electronic and structural orders, resembling the phase diagram of the pseudogap in cuprates [72]. In descending from the high temperature phase, the charge order emerges as a preemptive order, followed by an orbital selective Mott state (OSMT). As the temperature is further lowered to the metal-to-insulator transition temper-

ature  $T_{MIT}$ , the electronic CDW/OSMT order is further intertwined with the partial Peierls instability of the M<sub>2</sub> structure, and eventually, vanishes in the M<sub>1</sub> structure with full dimerization. This indicates that strain-engineered, thin-film VO<sub>2</sub> is indeed a strongly correlated system whose correlation can be modulated.

**Conclusion** — By interrogating the role of non-local correlations in epitaxially strained VO<sub>2</sub> with first principles plus experimental probes, we find emergent charge order deep in the metallic phase. The existence of non-degenerate vanadium positions induced by strain and enhanced by correlation attests to the importance of Mott physics in the complete phase diagram of thin-film VO<sub>2</sub>. Although rutile VO<sub>2</sub> under the largest strain enabled by a TiO<sub>2</sub> substrate cannot become a canonical Mott insulator, electron-electron interactions still result in novel electronic states like orbital selective Mott states and charge order, hallmarks of the strongly correlated system. Exciting future applications of the VO<sub>2</sub> transition rest on whether or not there exists a fast electronic transition with less reliance on structural transitions, and our work quantifies the strain effects in epitaxially grown thin films. The [001] growth orientation is most bulk like based on occupancy of the *d*-manifold and absorption lines, while the [001] and [110] begin to show en-

hanced correlation effects and spectral features. All of these aspects could have an important impact on designing next generation memristors utilizing the metal-to-insulator transition of quantum materials.

## ACKNOWLEDGMENTS

This work was supported by the Air Force Office of Scientific Research Multi-Disciplinary Research Initiative (MURI) entitled, Cross-disciplinary Electronic-ionic Research Enabling Biologically Realistic Autonomous Learning (CEREBRAL), under Award No. FA9550-18-1-0024 administered by Dr. Ali Sayir. We acknowledge

Diamond Light Source for time on Beamline I09 under Proposals SI25355 and SI13812 for XAS measurements. For the film synthesis we acknowledge support from the National Science Foundation [Platform for the Accelerated Realization, Analysis, and Discovery of Interface Materials (PARADIM)] under Cooperative Agreement No. DMR-1539918. Substrate preparation was performed in part at the Cornell NanoScale Facility, a member of the National Nanotechnology Coordinated Infrastructure (NNCI), which is supported by the National Science Foundation (Grant No. ECCS-1542081). We acknowledge Drs Tien-Lin Lee and Nicholas Quackenbush assistance with the XAS measurements at beamline I09 Diamond Light Source.

- 
- [1] S. Acharya, C. Weber, E. Plekhanov, D. Pashov, A. Taraphder, and M. Van Schilfgaarde, Metal-insulator transition in copper oxides induced by apex displacements, *Phys. Rev. X* **8**, 021038 (2018).
- [2] M. Yang, Y. Yang, B. Hong, L. Wang, K. Hu, Y. Dong, H. Xu, H. Huang, J. Zhao, H. Chen, *et al.*, Suppression of structural phase transition in  $\text{VO}_2$  by epitaxial strain in vicinity of metal-insulator transition, *Scientific reports* **6**, 23119 (2016).
- [3] Y. Kalcheim, N. Butakov, N. M. Vargas, M.-H. Lee, J. del Valle, J. Trastoy, P. Salev, J. Schuller, and I. K. Schuller, Robust coupling between structural and electronic transitions in a mott material, *Phys. Rev. Lett.* **122**, 057601 (2019).
- [4] Z. Shao, X. Cao, H. Luo, and P. Jin, Recent progress in the phase-transition mechanism and modulation of vanadium dioxide materials, *NPG Asia Materials* **10**, 581 (2018).
- [5] Z. Yang, C. Ko, and S. Ramanathan, Oxide electronics utilizing ultrafast metal-insulator transitions, *Annual Review of Materials Research* **41**, 337 (2011).
- [6] M. Yamamoto, R. Nouchi, T. Kanki, A. N. Hattori, K. Watanabe, T. Taniguchi, K. Ueno, and H. Tanaka, Gate-tunable thermal metal-insulator transition in  $\text{VO}_2$  monolithically integrated into a wse2 field-effect transistor, *ACS applied materials & interfaces* **11**, 3224 (2019).
- [7] J. Lappalainen, J. Mizsei, and M. Huotari, Neuromorphic thermal-electric circuits based on phase-change  $\text{VO}_2$  thin-film memristor elements, *Journal of Applied Physics* **125**, 044501 (2019).
- [8] W. Yi, K. K. Tsang, S. K. Lam, X. Bai, J. A. Crowell, and E. A. Flores, Biological plausibility and stochasticity in scalable  $\text{VO}_2$  active memristor neurons, *Nature communications* **9**, 4661 (2018).
- [9] A. Rana, C. Li, G. Koster, and H. Hilgenkamp, Resistive switching studies in  $\text{VO}_2$  thin films, *Scientific Reports* **10**, 1 (2020).
- [10] V. Eyert, The metal-insulator transitions of  $\text{VO}_2$ : A band theoretical approach, *Annalen der Physik* **11**, 650 (2002).
- [11] Z. Hiroi, Structural instability of the rutile compounds and its relevance to the metal-insulator transition of  $\text{VO}_2$ , *Progress in Solid State Chemistry* **43**, 47 (2015).
- [12] R. Rana, J. M. Klopff, J. Grenzer, H. Schneider, M. Helm, and A. Pashkin, Nonthermal nature of photoinduced insulator-to-metal transition in  $\text{nBO}_2$ , *Phys. Rev. B* **99**, 041102 (2019).
- [13] M. J. Wahila, G. Paez, C. N. Singh, A. Regoutz, S. Salliss, M. J. Zuba, J. Rana, M. B. Tellekamp, J. E. Boschker, T. Markurt, J. E. N. Swallow, L. A. H. Jones, T. D. Veal, W. Yang, T.-L. Lee, F. Rodolakis, J. T. Sadowski, D. Prendergast, W.-C. Lee, W. A. Doolittle, and L. F. J. Piper, Evidence of a second-order peierls-driven metal-insulator transition in crystalline  $\text{nBO}_2$ , *Phys. Rev. Materials* **3**, 074602 (2019).
- [14] D. B. Rogers, R. D. Shannon, A. W. Sleight, and J. L. Gillson, Crystal chemistry of metal dioxides with rutile-related structures, *Inorganic Chemistry* **8**, 841 (1969).
- [15] M. Imada, A. Fujimori, and Y. Tokura, Metal-insulator transitions, *Rev. Mod. Phys.* **70**, 1039 (1998).
- [16] R. M. Wentzcovitch, W. W. Schulz, and P. B. Allen,  $\text{VO}_2$ : Peierls or mott-hubbard? a view from band theory, *Phys. Rev. Lett.* **72**, 3389 (1994).
- [17] J. M. Booth and P. S. Casey, Anisotropic structure deformation in the  $\text{VO}_2$  metal-insulator transition, *Phys. Rev. Lett.* **103**, 086402 (2009).
- [18] H.-T. Kim, Y. W. Lee, B.-J. Kim, B.-G. Chae, S. J. Yun, K.-Y. Kang, K.-J. Han, K.-J. Yee, and Y.-S. Lim, Monoclinic and correlated metal phase in  $\text{VO}_2$  as evidence of the mott transition: Coherent phonon analysis, *Phys. Rev. Lett.* **97**, 266401 (2006).
- [19] M. M. Qazilbash, M. Brehm, B.-G. Chae, P.-C. Ho, G. O. Andreev, B.-J. Kim, S. J. Yun, A. Balatsky, M. Maple, F. Keilmann, *et al.*, Mott transition in  $\text{VO}_2$  revealed by infrared spectroscopy and nano-imaging, *Science* **318**, 1750 (2007).
- [20] M. M. Qazilbash, A. A. Schafgans, K. S. Burch, S. J. Yun, B. G. Chae, B. J. Kim, H. T. Kim, and D. N. Basov, Electrodynamics of the vanadium oxides  $\text{VO}_2$  and  $\text{V}_2\text{O}_3$ , *Phys. Rev. B* **77**, 115121 (2008).
- [21] S. Lee, K. Hippalgaonkar, F. Yang, J. Hong, C. Ko, J. Suh, K. Liu, K. Wang, J. J. Urban, X. Zhang, *et al.*, Anomalously low electronic thermal conductivity in metallic vanadium dioxide, *Science* **355**, 371 (2017).
- [22] D. Lee, B. Chung, Y. Shi, G.-Y. Kim, N. Campbell, F. Xue, K. Song, S.-Y. Choi, J. Podkaminer, T. Kim, *et al.*, Isostructural metal-insulator transition in  $\text{VO}_2$ , *Science* **362**, 1037 (2018).
- [23] T. Lin and Y. Zhang, Metal-insulator transition of mon-

- oclinic  $\text{VO}_2$  thin film without peierls distortion, *Vacuum* **163**, 338 (2019).
- [24] I. Kylänpää, Y. Luo, O. Heinonen, P. R. C. Kent, and J. T. Krogel, Compton profile of  $\text{VO}_2$  across the metal-insulator transition: Evidence of a non-fermi liquid metal, *Phys. Rev. B* **99**, 075154 (2019).
- [25] M. W. Haverkort, Z. Hu, A. Tanaka, W. Reichelt, S. V. Streltsov, M. A. Korotin, V. I. Anisimov, H. H. Hsieh, H.-J. Lin, C. T. Chen, D. I. Khomskii, and L. H. Tjeng, Orbital-assisted metal-insulator transition in  $\text{VO}_2$ , *Phys. Rev. Lett.* **95**, 196404 (2005).
- [26] T. C. Koethe, Z. Hu, M. W. Haverkort, C. Schüßler-Langeheine, F. Venturini, N. B. Brookes, O. Tjernberg, W. Reichelt, H. H. Hsieh, H.-J. Lin, C. T. Chen, and L. H. Tjeng, Transfer of spectral weight and symmetry across the metal-insulator transition in  $\text{VO}_2$ , *Phys. Rev. Lett.* **97**, 116402 (2006).
- [27] S. Biermann, A. Poteryaev, A. I. Lichtenstein, and A. Georges, Dynamical singlets and correlation-assisted peierls transition in  $\text{VO}_2$ , *Phys. Rev. Lett.* **94**, 026404 (2005).
- [28] C. Weber, D. D. O'Regan, N. D. M. Hine, M. C. Payne, G. Kotliar, and P. B. Littlewood, Vanadium dioxide: A peierls-mott insulator stable against disorder, *Phys. Rev. Lett.* **108**, 256402 (2012).
- [29] T. L. Cocker, L. V. Titova, S. Fourmaux, G. Holloway, H.-C. Bandulet, D. Brassard, J.-C. Kieffer, M. A. El Khakani, and F. A. Hegmann, Phase diagram of the ultrafast photoinduced insulator-metal transition in vanadium dioxide, *Phys. Rev. B* **85**, 155120 (2012).
- [30] S. Kim, K. Kim, C.-J. Kang, and B. I. Min, Correlation-assisted phonon softening and the orbital-selective peierls transition in  $\text{VO}_2$ , *Phys. Rev. B* **87**, 195106 (2013).
- [31] W. H. Brito, M. C. O. Aguiar, K. Haule, and G. Kotliar, Metal-insulator transition in  $\text{VO}_2$ : A DFT + DMFT perspective, *Phys. Rev. Lett.* **117**, 056402 (2016).
- [32] J. del Valle, P. Salev, Y. Kalcheim, and I. K. Schuller, A caloritronics-based mott neuristor, *arXiv preprint arXiv:1903.01062* (2019).
- [33] Y. Kalcheim, A. Camjayi, J. del Valle, P. Salev, M. Rozenberg, and I. K. Schuller, *Non-thermal resistive switching in mott insulators* (2019), *arXiv:1908.08555*.
- [34] T. Driscoll, H.-T. Kim, B.-G. Chae, M. Di Ventra, and D. Basov, Phase-transition driven memristive system, *Applied physics letters* **95**, 043503 (2009).
- [35] D. B. Strukov, G. S. Snider, D. R. Stewart, and R. S. Williams, The missing memristor found, *nature* **453**, 80 (2008).
- [36] J. Von Neumann, First draft of a report on the edvac, *IEEE Annals of the History of Computing* **15**, 27 (1993).
- [37] J. del Valle, P. Salev, F. Tesler, N. M. Vargas, Y. Kalcheim, P. Wang, J. Trastoy, M.-H. Lee, G. Kassabian, J. G. Ramírez, *et al.*, Subthreshold firing in mott nanodevices, *Nature* **569**, 388 (2019).
- [38] J. Laverock, A. R. H. Preston, D. Newby, K. E. Smith, S. Sallis, L. F. J. Piper, S. Kittiwatanakul, J. W. Lu, S. A. Wolf, M. Leandersson, and T. Balasubramanian, Photoemission evidence for crossover from peierls-like to mott-like transition in highly strained  $\text{VO}_2$ , *Phys. Rev. B* **86**, 195124 (2012).
- [39] H. Paik, J. a. Moyer, T. Spila, J. W. Tashman, J. a. Mundy, E. Freeman, N. Shukla, J. M. Lapano, R. Engel-Herbert, W. Zander, J. Schubert, D. a. Muller, S. Datta, P. Schiffer, and D. G. Schlom, Transport properties of ultra-thin  $\text{VO}_2$  films on (001)  $\text{TiO}_2$  grown by reactive molecular-beam epitaxy, *Appl. Phys. Lett.* **107**, 163101 (2015).
- [40] N. F. Quackenbush, H. Paik, J. C. Woicik, D. A. Arena, D. G. Schlom, and L. F. J. Piper, X-Ray Spectroscopy of Ultra-Thin Oxide/Oxide Heteroepitaxial Films: A Case Study of Single-Nanometer  $\text{VO}_2/\text{TiO}_2$ , *Materials* **2**, 5452 (2015).
- [41] S. Mukherjee, N. F. Quackenbush, H. Paik, C. Schlueter, T.-L. Lee, D. G. Schlom, L. F. J. Piper, and W.-C. Lee, Tuning a strain-induced orbital selective mott transition in epitaxial  $\text{VO}_2$ , *Phys. Rev. B* **93**, 241110 (2016).
- [42] N. F. Quackenbush, H. Paik, M. J. Wahila, S. Sallis, M. E. Holtz, X. Huang, A. Ganose, B. J. Morgan, D. O. Scanlon, Y. Gu, F. Xue, L.-Q. Chen, G. E. Sterbinsky, C. Schlueter, T.-L. Lee, J. C. Woicik, J.-H. Guo, J. D. Brock, D. A. Muller, D. A. Arena, D. G. Schlom, and L. F. J. Piper, Stability of the  $m_2$  phase of vanadium dioxide induced by coherent epitaxial strain, *Phys. Rev. B* **94**, 085105 (2016).
- [43] W.-C. Lee, M. J. Wahila, S. Mukherjee, C. N. Singh, T. Eustance, A. Regoutz, H. Paik, J. E. Boschker, F. Rodolakis, T.-L. Lee, *et al.*, Cooperative effects of strain and electron correlation in epitaxial  $\text{VO}_2$  and  $\text{nbo}_2$ , *Journal of Applied Physics* **125**, 082539 (2019).
- [44] A. D'Elia, S. Rezvani, A. Cossaro, M. Stredansky, C. Grazioli, B. W. Li, C. Zou, M. Coreno, and A. Marcelli, Strain induced orbital dynamics across the metal insulator transition in thin  $\text{VO}_2/\text{TiO}_2$  (001) films, *Journal of Superconductivity and Novel Magnetism* **10.1007/s10948-019-05378-0** (2020).
- [45] B. Lazarovits, K. Kim, K. Haule, and G. Kotliar, Effects of strain on the electronic structure of  $\text{VO}_2$ , *Phys. Rev. B* **81**, 115117 (2010).
- [46] S. Niitaka, H. Ohsumi, K. Sugimoto, S. Lee, Y. Oshima, K. Kato, D. Hashizume, T. Arima, M. Takata, and H. Takagi,  $a$ -type antiferro-orbital ordering with  $i_4/a$  symmetry and geometrical frustration in the spinel vanadate  $\text{MgV}_2\text{O}_4$ , *Phys. Rev. Lett.* **111**, 267201 (2013).
- [47] S. Guan, A. Rougier, M. R. Suchomel, N. Penin, K. Boudiang, and M. Gaudon, Geometric considerations of the monoclinic-rutile structural transition in  $\text{VO}_2$ , *Dalton Transactions* (2019).
- [48] A. Zylbersztein and N. F. Mott, Metal-insulator transition in vanadium dioxide, *Phys. Rev. B* **11**, 4383 (1975).
- [49] Z. Zhu and U. Schwingenschlögl, Comprehensive picture of  $\text{VO}_2$  from band theory, *Phys. Rev. B* **86**, 075149 (2012).
- [50] I. Kylänpää, J. Balachandran, P. Ganesh, O. Heinonen, P. R. C. Kent, and J. T. Krogel, Accuracy of ab initio electron correlation and electron densities in vanadium dioxide, *Phys. Rev. Materials* **1**, 065408 (2017).
- [51] A. S. Belozero, M. A. Korotin, V. I. Anisimov, and A. I. Poteryaev, Monoclinic  $M_1$  phase of  $\text{VO}_2$ : Mott-hubbard versus band insulator, *Phys. Rev. B* **85**, 045109 (2012).
- [52] M. C. Sánchez, G. Subías, J. García, and J. Blasco, Cooperative jahn-teller phase transition in  $\text{LaMnO}_3$  studied by x-ray absorption spectroscopy, *Phys. Rev. Lett.* **90**, 045503 (2003).
- [53] M. Medarde, C. Dallera, M. Grioni, B. Delley, F. Vernay, J. Mesot, M. Sikora, J. A. Alonso, and M. J. Martínez-Lope, Charge disproportionation in  $r\text{MnO}_3$  perovskites ( $r$  = rare earth) from high-resolution x-ray absorption spectroscopy, *Phys. Rev. B* **80**, 245105 (2009).
- [54] K. Momma and F. Izumi, *VESTA3* for three-dimensional

- visualization of crystal, volumetric and morphology data, *Journal of Applied Crystallography* **44**, 1272 (2011).
- [55] M. Sambi, M. Della Negra, and G. Granozzi, Growth and structural characterisation of vanadium oxide ultrathin films on tio2 (110), *Thin Solid Films* **400**, 26 (2001).
- [56] A. O'Hara and A. A. Demkov, Nature of the metal-insulator transition in Nbo<sub>2</sub>, *Phys. Rev. B* **91**, 094305 (2015).
- [57] P. Blaha, K. Schwarz, G. K. H. Madsen, D. Kvasnicka, and J. Luitz, *WIEN2K, An Augmented Plane Wave + Local Orbitals Program for Calculating Crystal Properties* (Karlheinz Schwarz, Techn. Universität Wien, Austria, 3-9501031-1-2).
- [58] J. P. Perdew, K. Burke, and M. Ernzerhof, Generalized gradient approximation made simple, *Phys. Rev. Lett.* **77**, 3865 (1996).
- [59] D. Koller, F. Tran, and P. Blaha, Improving the modified becke-johnson exchange potential, *Phys. Rev. B* **85**, 155109 (2012).
- [60] J. Sun, A. Ruzsinszky, and J. P. Perdew, Strongly constrained and appropriately normed semilocal density functional, *Phys. Rev. Lett.* **115**, 036402 (2015).
- [61] Y. Quan, V. Pardo, and W. E. Pickett, Formal valence, 3d-electron occupation, and charge-order transitions, *Phys. Rev. Lett.* **109**, 216401 (2012).
- [62] R. S. Mulliken, Electronic population analysis on leaomolecular wave functions. i, *The Journal of Chemical Physics* **23**, 1833 (1955).
- [63] R. F. Bader, Atoms in molecules, *Accounts of Chemical Research* **18**, 9 (1985).
- [64] F. L. Hirshfeld, Bonded-atom fragments for describing molecular charge densities, *Theoretica chimica acta* **44**, 129 (1977).
- [65] D. J. Singh and L. Nordstrom, *Planewaves, Pseudopotentials, and the LAPW method* (Springer Science & Business Media, 2006).
- [66] W. Atkinson, A. P. Kampf, and S. Bulut, Charge order in the pseudogap phase of cuprate superconductors, *New Journal of Physics* **17**, 013025 (2015).
- [67] M. Vojta and S. Sachdev, Charge order, superconductivity, and a global phase diagram of doped antiferromagnets, *Phys. Rev. Lett.* **83**, 3916 (1999).
- [68] A. Damascelli, Z. Hussain, and Z.-X. Shen, Angle-resolved photoemission studies of the cuprate superconductors, *Rev. Mod. Phys.* **75**, 473 (2003).
- [69] S. A. Kivelson, I. P. Bindloss, E. Fradkin, V. Oganesyan, J. M. Tranquada, A. Kapitulnik, and C. Howald, How to detect fluctuating stripes in the high-temperature superconductors, *Rev. Mod. Phys.* **75**, 1201 (2003).
- [70] P. A. Lee, N. Nagaosa, and X.-G. Wen, Doping a mott insulator: Physics of high-temperature superconductivity, *Rev. Mod. Phys.* **78**, 17 (2006).
- [71] K. Rossnagel, On the origin of charge-density waves in select layered transition-metal dichalcogenides, *Journal of Physics: Condensed Matter* **23**, 213001 (2011).
- [72] E. Fradkin, S. A. Kivelson, and J. M. Tranquada, Colloquium: Theory of intertwined orders in high temperature superconductors, *Rev. Mod. Phys.* **87**, 457 (2015).